Effects of Free Volume in Thin-Film Composite Membranes on Osmotic Power Generation

ARTICLE *in* AICHE JOURNAL · DECEMBER 2013

Impact Factor: 2.75 · DOI: 10.1002/aic.14217

2 AUTHORS, INCLUDING:

Tai-Shung Chung
National University of Singapore
726 PUBLICATIONS **19,494** CITATIONS

SEE PROFILE

Effects of Free Volume in Thin-Film Composite Membranes on Osmotic Power Generation

Xue Li and Tai-Shung Chung
NUS Graduate School for Integrative Science and Engineering, National University of Singapore, Singapore 117456, Singapore

Tai-Shung Chung
Dept. of Chemical and Biomolecular Engineering, National University of Singapore, Singapore 117576, Singapore

DOI 10.1002/aic.14217
Published online September 6, 2013 in Wiley Online Library (wileyonlinelibrary.com)

For the first time, the effects of free volume in thin-film composite (TFC) membranes on membrane performance for forward osmosis and pressure retarded osmosis (PRO) processes were studied in this work. To manipulate the free volume in the TFC layer, a bulky monomer (i.e., p-xylylenediamine) was blended into the interfacial polymerization and methanol immersion was conducted to swell up the TFC layer. Results from positron annihilation lifetime spectroscopy (PALS) show that p-xylylenediamine blending and methanol induced swelling enlarge and broaden the free volume cavity. In addition, the performance of TFC membranes consisting of different free volumes were examined in terms of water flux, reverse salt flux, and power density under high pressure PRO operations. The TFC-B-5 membrane (i.e., a TFC membrane made of blending monomers) with a moderate free volume shows the highest power density of 6.0 W/m^2 at 9 bar in comparison of TFC membranes with other free volumes. After PRO operations, it is found that the free volume of TFC layers decreases due to high pressure compression, but membrane transport properties in terms of water and salt permeability increase. Interestingly, the membrane performance in terms of resistance against high pressures and power density stay the same. A slow positron beam was used to investigate the microstructure changes of the TFC layer after PRO operations. Compaction in free volume occurs and the TFC layer becomes thinner under PRO tests but no visible defects can be observed by both scanning electronic microscopy and PALS. © 2013 American Institute of Chemical Engineers *AIChE J*, 59: 4749–4761, 2013

Keywords: free volume, osmotic power generation, thin-film composite membrane, pressure retarded osmosis

Introduction

Pressure retarded osmosis (PRO) is a membrane-based technology that harvests the energy of mixing two solutions from different salinity and converts it to electricity with the aid of a semipermeable PRO membrane and a hydroturbine. In addition, to utilize seawater and river water as the feed pair, the PRO process can use highly concentrated reverse osmosis (RO) retentate and recycled municipal wastewater as the feed pair for power generation.[1,2] By doing so, not only can the environmental issue such as the disposal of RO retentate be solved, but also produce much higher osmotic energy. Therefore, the development of PRO membranes for osmotic power generation will have repercussion effects on the production of both clean energy and clean water.

Loeb et al. conducted the first exploitation of osmotic power via PRO processes about 40 years ago.[3,4] Most early works on PRO was discontinued due to the absence of suitable PRO membranes.[5,6] The commercialization of forward osmosis (FO) membranes by Hydration Technology Innovations[7] and the set up of a PRO pilot for power generation by Statkraft[8,9] revived R & D for both FO and PRO. To date, significant advances on FO membranes[10–21] and their applications for water reuse[22–29] and osmotic power generation[30–35] have been made. So far, PRO membranes made from the thin-film composite (TFC) approach show the most promising results. The resultant TFC membranes consist of (1) an ultrathin cross-linked polymer synthesized from interfacial polymerization and (2) a porous substrate. The former acts as the primary barrier to salt and is responsible for the water flux across the membrane to generate power, whereas the latter provides the cushion for the TFC layer and the mechanical support against the hydraulic pressure. However, most TFC membranes for PRO suffer severe performance deterioration due to irreversible deformation and damage on both TFC and supporting layers caused by the high pressure at the seawater side.[35] As a result, most TFC membranes show low power densities in actual PRO tests. Hence, a fundamental understanding of (1) membrane structural changes and (2) membrane performance changes under high pressures is critical for further improvements of TFC membranes for PRO processes.

Additional Supporting Information may be found in the online version of this article.

Correspondence concerning this article should be addressed to: T. S. Chung, at chencts@nus.edu.sg.

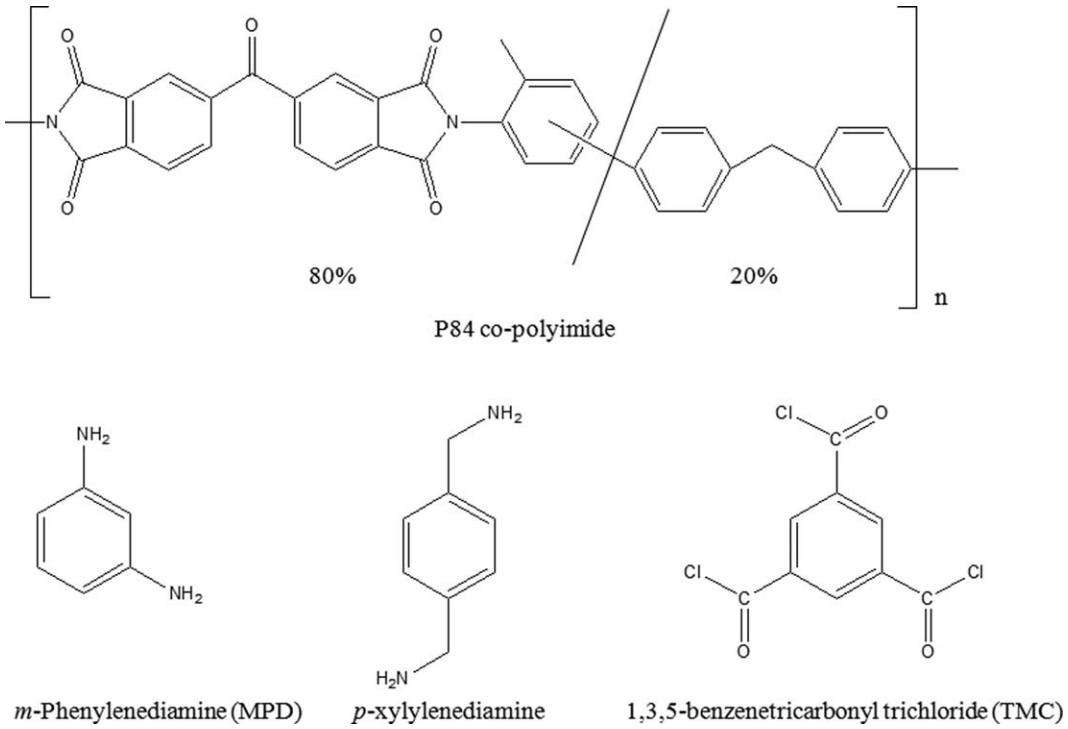

Figure 1. Chemical structure of P84 copolyimide (referred to as PI) and monomers of TFC membranes.

As the TFC layer is the portion essentially responsible for the transport properties of water and salt, its separation performance can be closely estimated by its free volume, one of the most important characteristics of thin films.[36–41] The free volume of the TFC layer may be possibly adjusted by various means including (1) the employment of different amines and acyl halides for the interfacial polymerization, (2) the changes of reaction conditions such as monomer concentrations, duration, temperature, solvent systems, and (3) physical and chemical post-treatments. As the osmotic power generation is a product of water flux and transmembrane pressure, and the water flux is strongly dependent on inherent water and salt permeability across the membrane, by tuning the free volume of the TFC layer, one may obtain a PRO membrane with desired properties for PRO processes. To the best of our knowledge, there is very limited information available in the literature on the variation of free volume in TFC membranes and how the free volume influences the membrane performance for PRO operations. Therefore, the objective of this work is to investigate and present an in-depth understanding of the relationship between the free volume in the TFC layer and membrane performance for osmotic power generation.

A series of experiments is designed and carried out to investigate the behavior and the respective effects of the TFC layer in a PRO operation. First, the free volume of the TFC layer is tuned with approaches such as blending with bulky monomers and swelling with methanol, positron annihilation lifetime spectroscopy (PALS) is then used to quantitatively characterize the free volume changes. After that, their respective effects on membrane FO and PRO performance would be measured and correlated. It is envisioned that this fundamental study not only opens up new insights on the relationship among free volume, structural change and power density for TFC membranes under PRO operations, but also provides useful strategies to design better PRO membranes.

Experimental

Materials and chemicals

P84 copolyimide (referred to as polyimide (PI) thereafter) (BTDA-TDI/MDI, copolyimide of 3, 3′, 4, 4′-benzophenone tetracarboxylic dianhydride and 80% methylphenylene diamine + 20% methylene diamine) was purchased from HP Polymer, Austria. The chemical structure is shown in Figure 1. The solvent *N*-methyl-2-pyrrolodinone (>99.5%) and nonsolvent ethylene glycol (EG, 99.9%) were purchased from Merck and VWR, respectively, and were used to prepare the casting solutions. The deionized water used in experiments was produced by a Milli-Q ultrapure water system (Millipore). *m*-Phenylenediamine (MPD, >99%) and 1,3,5-benzenetricarbonyl trichloride (TMC, 98%) were purchased from Sigma–Aldrich Chemical Co. *p*-Xylylenediamine (>99%) was purchased from Tokyo Chemical Industry. Hexane, methanol, and sodium chloride (NaCl) were purchased from Merck. All chemicals were used as received.

Fabrication of PI membranes

The PI membranes were prepared by the Loeb-Sourirajan wet-phase inversion method. Prior to dope preparation, the PI polymer was dried overnight at 90 ± 5°C in a vacuum oven (2 mbar) to remove moisture content. Four types of casting solutions were prepared and designated to be PI-1 to PI-4, as summarized in Table 1. The PI membranes were prepared with a casting knife of 60 μm thickness. After being peeled off from the casting glass plate, the resultant membranes were rinsed with tap water for 6 h to remove the residual solvent and EG.

Table 1. Compositions of PI Casting Solutions, the Porosity, PWP, and Mechanical Properties of As-Cast Membranes

Solution	Component (wt %)			EG/PI Ratio (wt/wt)	Porosity	PWP[a] (L m^{-2} h^{-1} bar^{1})	Mechanical Properties		
	PI	EG	NMP				Elongation at Break (%)	Tensile Strength (MPa)	Young's Modulus (MPa)
PI-1	25	0	75	0	61 ± 6	16 ± 1	24 ± 6	6.2 ± 0.8	248 ± 25
PI-2	22	5	73	0.23	65 ± 7	155 ± 14	13 ± 4	4.2 ± 0.4	194 ± 13
PI-2 (MeOH)[b]	–	–	–	–	–	–	13 ± 4	3.9 ± 0.6	182 ± 25
PI-3	21	10	69	0.48	66 ± 10	227 ± 13	10 ± 2	3.8 ± 0.4	163 ± 7
PI-4	20	15	65	0.75	70 ± 4	410 ± 45	3 ± 2	1.4 ± 0.6	155 ± 30

[a]The PWP was tested at a constant pressure of 1 bar.
[b]The PI-2 substrate was soaked in methanol for 12 h prior to tests.

Fabrication of PI-TFC membranes and post-treatments

The TFC polyamide membrane was synthesized on top of the PI porous membrane by interfacial polymerization using the following procedures: (1) the backside (i.e., porous side) of the PI membrane was sealed to ensure only the top side of the substrate being in contact with the solution; (2) the membrane substrate was placed in an aqueous solution of 0.1 mol L^{-1} MPD for 1.5 min except for the cases of TFC-B membranes. The TFC-B membranes used blends of diamine monomers for interfacial polymerization where 0.1 mol L^{-1} of MPD was blended with *p*-xylylenediamine in various ratios; (3) the excess diamine solution was poured off and the residual droplets on the substrate were removed by a rubber roller; (4) the substrate was then soaked in a hexane solution containing 0.2 wt % TMC for a 90-s interfacial polymerization followed by a 10-min air dry. Finally, the resultant membrane was washed thoroughly with deionized water. Some of the TFC membranes (i.e., TFC-MeOH membranes) were subjected to methanol swelling post-treatment where the membranes were soaked in methanol for 12 h, washed and stored in deionized water before tests.

Characterizations

Morphology, Porosity, and Mechanical Properties of Porous Membranes. The morphology of membranes was examined by scanning electronic microscopy (SEM JEOL JSM-5600LV) and field emission scanning electronic microscopy (FESEM, JEOL JSM-6700F). Before SEM/FESEM tests, samples were prepared in liquid nitrogen followed by platinum coating using a Jeol JFC-1100E ion sputtering device.

Membrane porosity was determined by testing the wet membrane weight, m_1 (g), and the dry membrane weight, m_2 (g). The membrane porosity can be calculated from Eq. 1

$$\varepsilon = \frac{(m_1 - m_2) \div \rho_w}{(m_1 - m_2) \div \rho_w + m_2 \div \rho_p} \times 100 \quad (1)$$

where ε, ρ_w, and ρ_p indicate the membrane porosity (%), density of water (g/cm^3), and density of polymer (g/cm^3), respectively.

Mechanical properties of membranes including the elongation at break, maximum tensile strength, and Young's modulus were measured at the constant elongation rate of 10 mm min^{-1} with a starting gauge length of 50 mm by an Instron tensiometer (Model 5542, Instron Corp.). Ten samples were tested to minimize the experimental error and ensure the accuracy.

Water Transport Properties.

$$J_w = A(\Delta\pi - \Delta P) \quad (2)$$

The water permeation flux, J_w is given by Eq. 2, where A is the water permeability coefficient of the membrane, $\Delta\pi$ is the osmotic pressure gradient across the membrane, and ΔP is the hydraulic pressure difference. Similarly, the salt flux across the membrane, J_s, can be written as

$$J_S = B\Delta C \quad (3)$$

where B is the salt permeability coefficient of the membrane, ΔC is the concentration difference. In this work, A, B, and salt rejection, R_s, were determined by testing the membranes under the RO mode in dead-end tests. The dead-end filtration setup with an effective membrane area of 7.06 cm^2 has been described clearly in our previous studies.[13,15] The testing temperature was at 24 ± 1°C. A was obtained from the pure water flux under a consistent pressure, ΔP, of 1.0 bar. The salt rejection, R_s, was tested under a transmembrane pressure of 1 bar using a 200 ppm NaCl feed solution based on conductivity measurements by a conductivity meter (Schott Instruments Gmbh, Germany). B, which is the intrinsic property of a membrane to retain salt, was derived from the solution-diffusion theory as follows[5,6]

$$B = A\frac{(1 - R_s)(\Delta P - \Delta\pi)}{R_s} \quad (4)$$

Determination of TFC membrane performance in FO tests. FO experiments conducted in this work were similar to those of our previous studies.[19,20] The membrane module consists of one water channel on each side of the membrane. No spacer was used in the testing. Both draw solution (i.e., synthetic RO retentate using NaCl solutions) and feed solution (i.e., deionized water) flowed counter-currently through the filtration cell and were recirculated during experiments. One membrane orientation was tested at 24 ± 1°C, with the selective layer against the draw solution (referred to as the PRO mode).

The water permeation flux, J_w (L m^{-2} h^{-1}, LMH), was calculated from Eq. 5

$$J_w = \frac{\Delta\omega}{\Delta t}\frac{1}{A_m} \quad (5)$$

where $\Delta\omega$ (kg) is the absolute weight change of feed solution over a predetermined time Δt (h) during the FO tests and A_m (m^2) is the effective membrane area.

The reverse salt flux, J_s (g m^{-2} h^{-1}, gMH) was determined from the salt concentration increment in the feed by measuring the conductivity change when deionized water was used as the feed solution

$$J_s = \frac{(C_t V_t) - (C_0 V_0)}{\Delta t}\frac{1}{A_m} \quad (6)$$

where C_t (mol L^{-1}) and V_t (L) are the salt concentration and the volume of the feed solution at time t, respectively; C_0

(mol L^{-1}) and V_0 (L) are the initial salt concentration and the volume of the feed solution, respectively.

Theoretically, the relationship between water flux and driving force in a FO process under the PRO mode can be described as Eq. 7[6,42]

$$J_w = \frac{1}{K_m} \ln \frac{A\pi_{D,m} - J_w + B}{A\pi_{F,b} + B} \quad (7)$$

where $\pi_{D,m}$ and $\pi_{F,b}$ are the osmotic pressures of the draw solution at the membrane surface and the bulk feed solution, respectively and K_m denotes the solute resistivity.

Similarly, Eq. 8 is applied to the FO mode

$$J_w = \frac{1}{K_m} \ln \frac{A\pi_{D,b} + B}{A\pi_{F,m} + J_w + B} \quad (8)$$

where $\pi_{D,b}$ is the osmotic pressure of the bulk draw solution and $\pi_{F,m}$ is the osmotic pressure of the feed solution at the membrane surface.

Determination of TFC membranes performance in PRO tests. The PRO tests for osmotic power generation were conducted on a lab-scale PRO setup using membrane modules as described in previous publications.[34,35] Similar to FO tests, model RO retentate (1 mol L^{-1} NaCl) and deionized water were used as draw and feed solutions, respectively. TFC membranes were oriented in the PRO configuration for all tests. Counter-current flows at 0.3 L/min were applied to both the draw solution and the feed solution, and a constant temperature of 24 ± 1°C was maintained. The power density is calculated by Eq. 9

$$W = J_w \Delta P \quad (9)$$

where ΔP is the hydraulic pressure difference across the membrane, and J_w is the water permeation flux that is determined either from experimental measurements in PRO tests, or theoretical calculation as

$$J_w = A\left[\pi_{D,b} \exp\left(-\frac{J_w}{k}\right) \frac{1}{1 + \frac{B}{J_w}[\exp(J_w K_m) - 1]} - \Delta P\right] \quad (10)$$

where $\pi_{D,b}$ is the osmotic pressure of the bulk draw solution; k refers to the mass transfer coefficient which has been clearly described in many other publications.[30,31]

Positron annihilation lifetime spectroscopy. PALS was used to characterize membranes and the details were described elsewhere.[36,37,43,44] The depth profile of membrane cavity was detected by Doppler broadening energy spectra (DBES) coupled with a slow positron beam. An HP Ge detector at a counting rate of approximately 4800 cps was used to record DBES, and the total number of counts for each spectrum was 1.0 million. S and R parameters are two important characteristic values to express DBES.[38] Results from the slow positron beam show the depth profile of membrane cavity as a function of incident position energy expressed in terms of depth (Eq. 11)

$$Z(E_+) = \frac{40}{\rho} E_+^{1.6} \quad (11)$$

where Z is the depth (nm), ρ denotes the density of the polymer (g/cm^3), and E_+ is the incident positron energy (keV).

The free volumes of polyamides membranes were probed by detecting the γ-rays (1.28 MeV) and the annihilation γ-rays (0.511 MeV) from the nuclear decay of a positron emission from the ^{22}Na positron source by the bulk PALS. The ^{22}Na isotope was used as the source of positrons and sealed in Kapton® films. Experiments were conducted in different incident positron energy. All data were analyzed into lifetime using the PATFIT program.[45]

Results and Discussion

Preferential polyimide porous substrates for PRO TFC membranes

As aforementioned, four types of PI porous substrates with different surface morphologies and bulk porosities have been prepared for the synthesis of TFC membranes. Experiments were carried out to investigate (1) the substrates' morphology, pure water permeability (PWP), and mechanical properties, (2) the TFC layers' morphology, FO performance, and free volume, (3) the TFC membranes' PRO performance at high pressures. We aim to reveal the relationship among substrate morphology, free volume of TFC layers, FO and PRO performance of TFC membranes, and to explore the preferential substrate and monomer compositions for PRO operations.

Morphology, PWP, and mechanical properties of porous membranes. Figure 2 displays the SEM images of PI substrates (from PI-1 to PI-4) cast from different solutions with an increasing ratio of EG to PI, as shown in Table 1. Glycol and its derivatives have been frequently used in the fabrication of asymmetric membranes.[46–48] By adjusting the EG amount in casting solutions, one may be able to manipulate the thermodynamics and kinetics of membrane formation via phase inversion as well as membrane morphology and porosity.[46] All four substrates show similar thicknesses and sponge-like morphologies. As compared with the PI-1 substrate, an increase in the EG/PI ratio results in an increase in both surface and bulk porosities. Initially, the bottom surfaces of PI-2 and PI-3 substrates become visibly porous, whereas the top surfaces maintain relatively dense. With a further increment in EG/PI ratio, as in the substrate PI-4, large surface pores appear on its top surface with sizes of hundred nanometers. In addition, different from other three PI substrates, a fully porous structure can be observed just beneath the top skin layer (Figure 2, PI-4-D). The PI-4 substrate with this morphology possesses the highest porosity of 70.3% among the four substrates. Clearly, EG acts as the pore-forming agent and causes the structure change. As a result, the PWP of the four PI substrates vary accordingly as listed in Table 1. The original PI-1 substrate has only a PWP of 16 ± 1 L m^{-2} h^{-1} bar^{-1} (LMH/bar). This value is greatly enhanced by factors of 9, 14, and 26 for substrates PI-2 (155 ± 14 LMH/bar), PI-3 (227 ± 13 LMH/bar), and PI-4 (410 ± 45 LMH/bar), respectively. As PRO membranes require a high water flux, substrates PI-2 to PI-4 with enhanced water permeabilities may be preferred as the porous substrates for the fabrication of TFC membranes.

Table 1 also summarizes the elongation at break, tensile strength, and Young's modulus of the four PI substrates. These mechanical properties all decrease gradually with increasing EG/PI ratio, which are attributed to the fact that the mechanical properties of a membrane can be weakened by lowering polymer concentration and increasing porosities. Moreover, it has been reported that the incorporation of glycol additives may decrease the rigidity of polymer

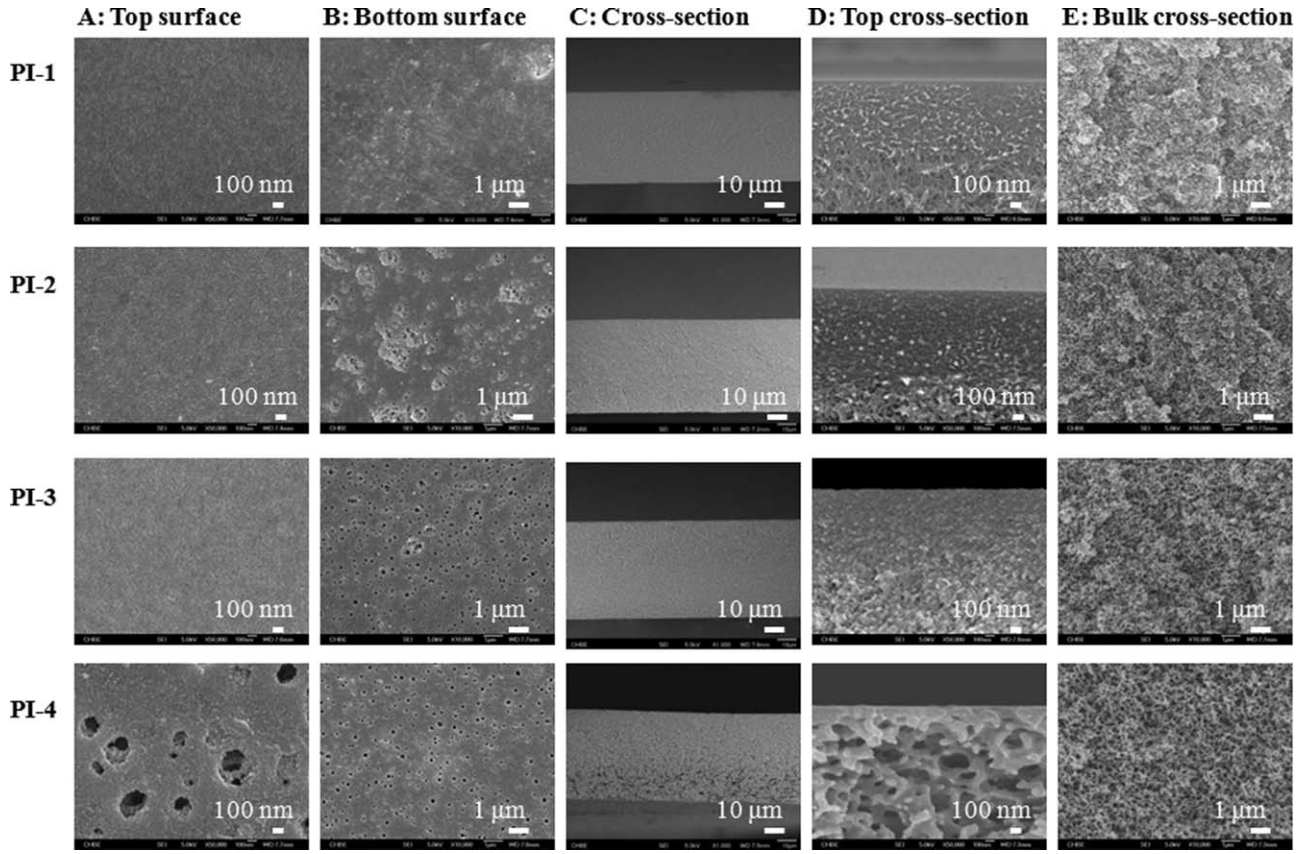

Figure 2. SEM morphologies of as-cast PI membranes.

(The membranes were cast on glass plates by using casting solutions of PI-1, PI-2, PI-3, and PI-4).

chains.[47,48] As a result, the PI membrane with a higher EG/PI ratio exhibits a lower mechanical strength.

Morphology and FO performance of TFC membranes. Figure 3 illustrates the top skin morphologies of TFC membranes fabricated on PI-1 to PI-4 porous substrates. The SEM images confirm the formation of TFC layers over the porous substrates. The TFC-PI-1 membrane has a top layer fully covered by small globular and worm-like domains. The domain sizes tend to widen for the TFC-PI-2 and TFC-PI-3 membranes, which may be due to the increased surface porosity with an increase in EG/PI ratio and the vigorous monomer migration during interfacial polymerization.[17] Visible defects are formed on top of the TFC-PI-4 membrane. This is due to the fact that the top surface of its porous substrate consists of pores with sizes of hundreds of nanometers, it is impossible to produce an intact and fully covered TFC layer over the whole substrate's surface. In other words, the interfacial polymerization may take place inside the porous substrate as the reaction reagents can penetrate into the bulk membrane through the big pores and form a TFC layer as a barrier within the PI substrate.[19]

Figure 4 presents the water fluxes and reverse salt fluxes of four TFC-PI membranes in conventional cross-flow FO tests where the TFC layer faced the draw solution. The TFC-PI-1 membrane has the lowest water flux and a low reverse salt flux because its substrate is not fully porous. By adjusting the dope composition with higher EG/PI ratios, the water fluxes of TFC-PI-2 and TFC-PI-3 membranes increase to $\sim$33 L m^{-2} h^{-1} (LMH) from 9 L m^{-2} h^{-1} of the original TFC-PI-1 membrane. Meanwhile, their reverse salt fluxes go up to 5–6 g m^{-2} h^{-1} (gMH) which is considered to be relatively low for osmosis membranes. Further increasing the EG/PI ratio induces a sudden decrease in water flux and a remarkable increase in reverse salt flux for the TFC-PI-4 membrane. It is possibly due to the fact that the TFC layer within the TFC-PI-4 membrane is defective and tortuous. There is an exacerbated internal concentration polarization inside the porous membrane matrix, hence the membrane performance deteriorates. In summary, TFC-PI-2 and TFC-PI-3 membranes have the comparable FO performance as compared with many other FO membranes reported elsewhere.[19] Taking into consideration that the PI-2 membrane has stronger mechanical properties than PI-3 in the power generation application where a high hydraulic pressure is used, it is chosen as the membrane substrate for the fabrication of TFC membranes with various free volumes in the subsequent studies.

Effects of free volume of TFC membranes

It is known that flux, permeability, and power density of various membranes can be significantly enhanced by alcohol treatments due to mechanisms such as solvent induced swelling,[49–51] removal of unreacted monomers, or thinning of the dense-selective layer.[34,52,53] The free volume of TFC membranes can also be tailored by blending with bulky moieties as monomers during the IP reaction.[54,55] Therefore, three TFC membranes were prepared and compared in order to investigate the effects of free volume on FO and PRO performance. They are (1) TFC-PI-2 membrane without any treatments, (2) TFC-MeOH membrane (i.e., the TFC-PI-2 membrane with methanol treatment as referred to Fabrication of PI-TFC membranes and post-treatments Section), and (3)

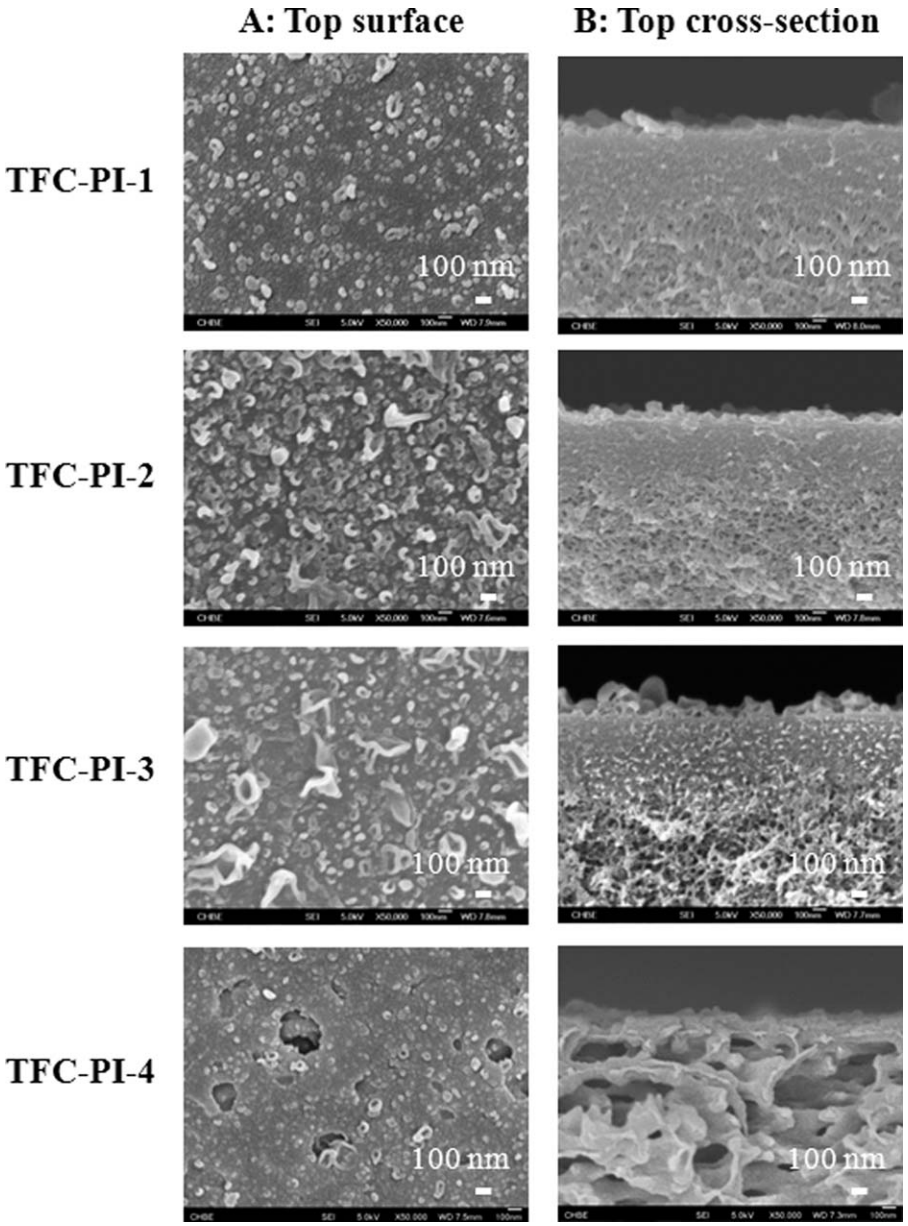

Figure 3. SEM images of top TFC-PI morphologies.

(The TFC layers were polymerized on substrates of PI-1, PI-2, PI-3, and PI-4. The membranes were air-dried for 10 min after interfacial polymerization).

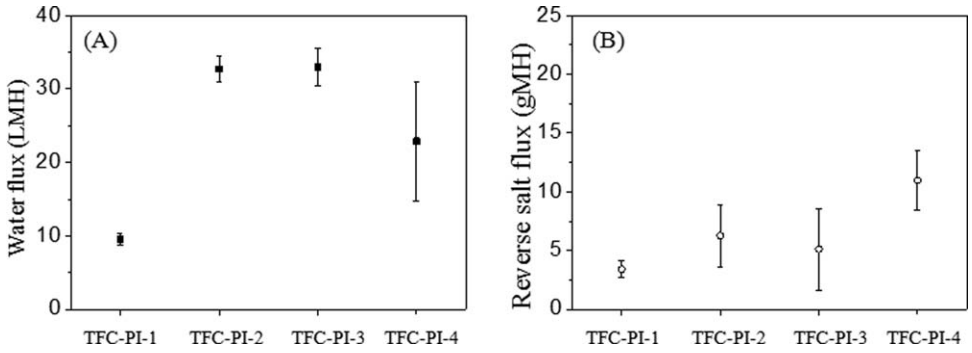

Figure 4. (A) Water flux and (B) reverse salt flux as a function of TFC-PI membranes.

(Conventional FO tests where the TFC layer faces the draw solution using deionized water as the feed solution and 1 M NaCl as the draw solution).

Table 2. *o*-Ps Lifetime, Intensity, and Free-Volume Radius of the Three Polyamides Thin-Film Membranes

Membrane ID	T_3 (ns)	I_3 (%)	Radius (Å)
TFC	1.60 ± 0.02	8.91 ± 0.25	2.45 ± 0.02
TFC-B-5	1.69 ± 0.02	7.32 ± 0.21	2.55 ± 0.02
TFC-MeOH	2.09 ± 0.02	15.24 ± 0.18	2.93 ± 0.01

TFC-B membranes (i.e., the TFC polyamide layer synthesized from mixed diamine monomers of MPD and *p*-xylylenediamine, as referred to Fabrication of PI-TFC membranes and post-treatments Section). For easy comparison, the last TFC membranes are denoted as "TFC-B-X" in which the "X" represents the loading percentage (i.e., mole concentration, %) of *p*-xylylenediamine. For example, TFC-B-1 refers to a TFC membrane made from a diamine mixture of 1 mol % *p*-xylylenediamine and 99 mol % MPD.

Supporting Information Table S1 shows the X-ray photoelectron spectroscopy (XPS) results of atomic ratios of [N]/[C] for TFC and TFC-B membranes, through which the successful incorporation of different ratios of *p*-xylylenediamine into the cross-linked polyamide network (i.e., the TFC layer) is verified. Thereafter, TFC layers with different degrees of cross-linking and free volumes have been synthesized with the aid of *p*-xylylenediamine. Supporting Information Figure S2 compares their FO performance and top surface morphologies as a function of *p*-xylylenediamine. By incorporating a small amount (i.e., 5%) of *p*-xylylenediamine into the TFC layer, water flux is enhanced accompanying with an acceptable reverse salt flux; however, a further increase in *p*-xylylenediamine content (i.e., 50%) results in a drop in water flux and a big jump in reverse salt flux. Hence, the TFC-B-5 membrane is chosen as the representative TFC membrane made of mixed monomers in the subsequent study.

Free Volume of TFC Membranes Probed by PALS. PALS is a powerful instrument capable of probing free volume of various polymers at the atomic level and providing information of free volume size and distribution.[56] However, due to the quenching effect of polar C═O groups in polyimides, it is almost impossible to obtain a practical PALS spectrum pertaining to *o*-Ps for TFC membranes based on polyimides substrates. Pure polyamide thin-film membranes without the polyimide substrates were, therefore, carefully prepared for more precise characterizations of free volume. The synthesis procedures of pure polyamide thin-film membranes are given in the Supporting Information. Table 2 summarizes the PALS results of these three polyamides membranes, while Figure 5 presents their free volume radius distributions calculated from the MELT program.[57] The pristine TFC membrane exhibits the smallest free volume radius with the narrowest distribution. In the blending monomer case, the TFC-B-5 membrane has a longer *o*-Ps lifetime and a higher free volume radius of 2.55 Å. An increment of approximately 4% in free volume radius is observed in the TFC-B-5 membrane mostly due to the bulkier molecular size of *p*-xylylenediamine, which interferes polymer chain packing and introduces a looser structure into the polyamide cross-linking network. Moreover, the free volume size distribution of the TFC-B-5 membrane is also broader, indicating that the polyamide formed from a mixture of moieties with different sizes of cross-linking cavities. Conversely, when the pristine TFC membrane is treated by methanol, a swelling effect is induced. The TFC-MeOH membrane shows remarkable increases in τ_3 and I_3, corresponding to the free volume size and concentration, respectively. The free volume radius of the TFC-MeOH membrane is enhanced by 20% comparing to the pristine TFC membrane. In addition, a bimodel lifetime distribution is found due to a new free volume (τ_3 ~1.1 ns) has been created as a result of swelling.[39] The PALS analyses indicate that (1) both blending and swelling treatments induce free volume increments and (2) the methanol induced swelling has a much bigger effect on free volume enlargement than blending a bulky *p*-xylylenediamine moiety into the TFC layer. As a result, the polyamide in the TFC-MeOH membrane is much looser. It would create more pathways for both water and salt transports across the membrane and subsequently affect the FO and PRO performance.

Effects of Free Volume of TFC Membranes on FO Performance. Table 3 summarizes the transport properties of the three TFC membranes under RO condition. The pristine membrane has the lowest water permeability, *A*, of 0.8 LMH/bar and salt permeability, *B*, of 0.10 LMH, whereas the TFC-B-5 membrane has an increased *A* value of 1.0 LMH/bar and an increased *B* value of 0.18 LMH owing to its bigger free volume size. The TFC-MeOH membrane demonstrates the highest water permeability (1.6 LMH/bar) and salt permeability (0.36 LMH). The intrinsic water permeability which is independent on dense layer thickness also increases in the order of TFC < TFC-B-5 < TFC-MeOH. This result suggests that (1) the loose structure of cross-linked polyamide layer and (2) the enlargements of free volume radius and its distribution may enhance the transport properties. One drawback associated with a bigger free volume is the deterioration of salt rejection. The salt rejection drops from 86% of the pristine membrane to 81% of the TFC-B-5 membrane, then further to 79% of the TFC-MeOH membrane due to the enlargements of free volume radius and distribution. These results agree well with previous findings that the water and salt transport is faster in dense membrane films with a large free volume.[40,41,58]

Figure 6 illustrates the morphological changes of the TFC membranes after the blending and methanol treatments. The

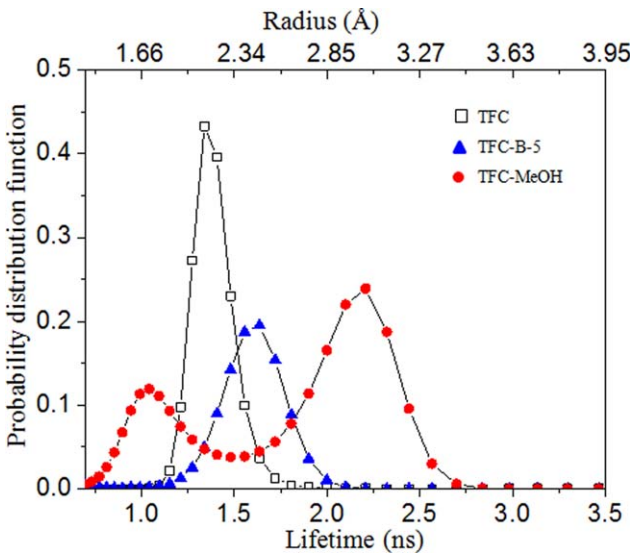

Figure 5. Free volume radius distributions of the three polyamides thin-film membranes.

[Color figure can be viewed in the online issue, which is available at wileyonlinelibrary.com.]

Table 3. Transport Properties of the Three TFC Membranes

Membrane		Water Permeability Coefficient, A (L m^{-2} h^{-1} bar^{-1})	Intrinsic Water Permeability[a] (L m^{-1} h^{-1} bar^{-1})	Salt Permeability Coefficient[b], B (L m^{-2} h^{-1})	Salt Rejection[b] (%)
TFC		0.8 ± 0.2	5.2×10^{-8}	0.10±0.03	86±4
TFC-B-5		1.0 ± 0.4	5.6×10^{-8}	0.18 ± 0.10	81 ± 8
TFC-MeOH		1.6 ± 0.2	8.2×10^{-8}	0.36 ± 0.09	79 ± 9
After PRO process	TFC	0.9 ± 0.2	5.2×10^{-8}	0.13 ± 0.01	84 ± 3
	TFC-B-5	1.2 ± 0.4	4.9×10^{-8}	0.26 ± 0.06	80 ± 2
	TFC-MeOH	1.9 ± 0.5	4.6×10^{-8}	0.63 ± 0.17	72 ± 10

[a]Intrinsic water permeability of the membrane is a product of water permeability and dense layer thickness (measured by PALS).
[b]200 ppm NaCl as the feed solution in RO tests under an applied pressure of 1 bar.

globular and worm-like domains on the original TFC membrane were obviously bloated after the methanol treatment. Clearly, swelling induced by methanol not only enlarges the microscopic free volume size but also affects the macroscopic morphology of the TFC membrane. In the case of blending treatment, the TFC layer becomes even flatter. This is mainly attributed to the fact that the bulkier moiety of *p*-xylylenediamine not only has a slower migration rate toward the TMC solution but also has a lower reactivity toward the interfacial polymerization. As a consequence, smaller domains are formed on top of the PI substrates, as elucidated by Li et al. on the formation mechanism of TFC membranes.[17]

The FO performance, in terms of water flux and reverse salt flux, are determined by the properties of both the selective layer and the porous substrate. As the TFC membranes in Figure 6 were made from the same substrate, the differences in their FO performance arise mainly from their TFC layers. As shown in Figure 6, the pristine TFC membrane has the lowest water flux among these three membranes at low draw solution concentrations (i.e., 0.5–1.0 M) but its flux keeps increasing almost linearly with increasing draw solution concentration and becomes the highest at the high draw solution concentration of 2.0 M. On the contrary, the TFC-MeOH membrane initially shows the highest water flux at low draw solution concentrations, but appears to level off quickly at a higher draw solution concentration of 2.0 M. For the TFC-B-5 membrane, a moderate water flux between the previous two cases is observed. The different relationship between water flux and draw solution concentration may be attributed to their different free volumes. The TFC-MeOH membrane has the highest free volume radius in its selective layer which facilitates both water and salt diffusivities and permeabilities.[40] As a result, it has the highest reverse salt flux of about 15–20 gMH higher than the other two TFC membranes at low draw solution concentrations. The gap continuously increases to ~30 gMH when the draw solution concentration reaches 2.0 M. The high reverse salt flux not only reduces the concentration gradient across the membrane but also significantly subdues the effective driving force for water transport through the membrane. Thus, the water flux of the TFC-MeOH membrane at a high draw solution concentration is severely impaired by its high reverse salt leakage. This phenomenon is less pronounced for the TFC-B-5 membrane because it has a moderate increment in free volume size and a slightly higher reverse salt flux comparing to

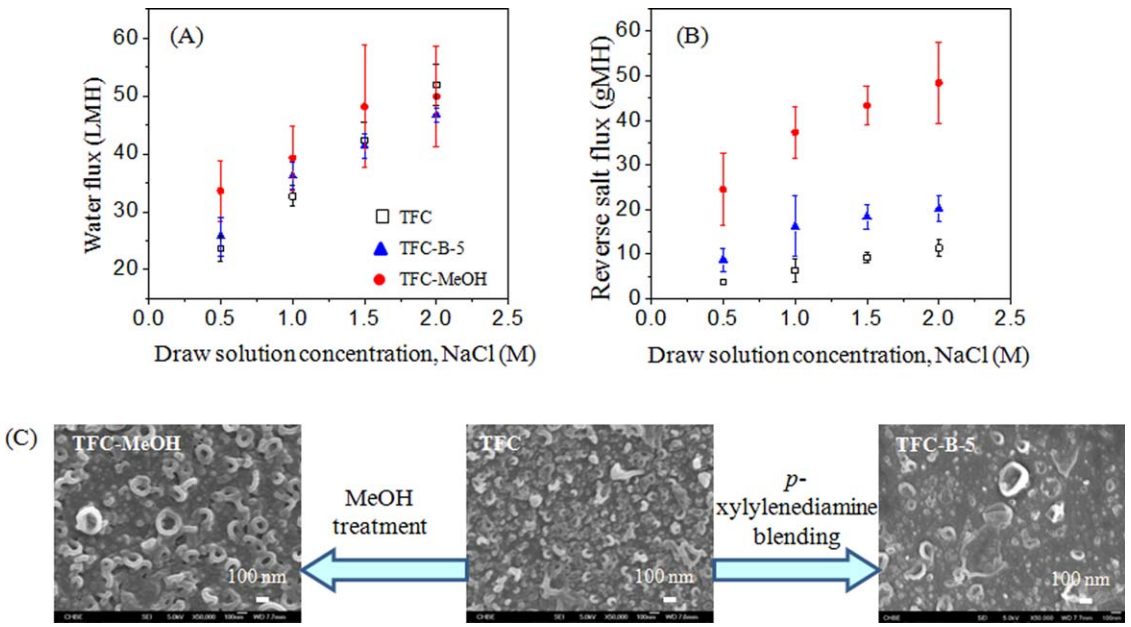

Figure 6. (A) Water flux and (B) reverse salt flux of TFC membranes under conventional FO tests using deionized water as the feed and (C) morphologies of the original TFC membrane (middle), the TFC-MeOH membrane (left), and the TFC-B-5 membrane without methanol treatment (right).

[Color figure can be viewed in the online issue, which is available at wileyonlinelibrary.com.]

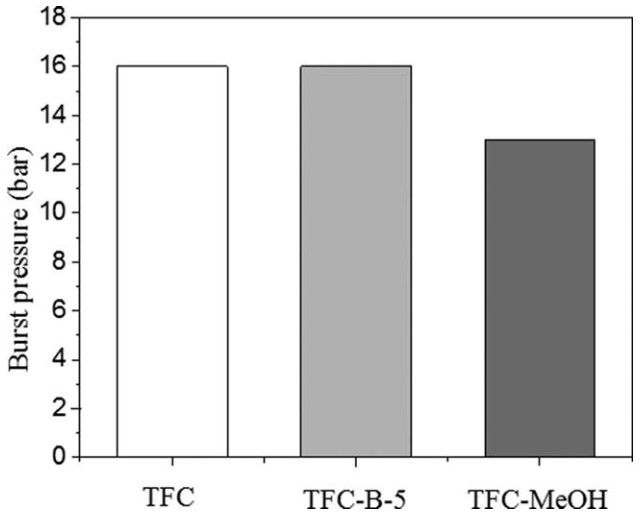

Figure 7. Burst pressures of the three TFC membranes in high pressure PRO processes.

(The burst pressure is defined as the point when the water flux flows reversely in high pressure PRO processes).

the TFC membrane. One may, therefore, conclude that the increase in free volume promotes water flux in FO processes while the free volume increment caused by mixed monomers makes a less unfavorable impact on reverse salt flux than that induced by methanol swelling.

Effects of Free Volume of TFC Membranes on High Pressure PRO Processes. Figure 7 shows the burst pressure of these three TFC membranes in high pressure PRO tests. The burst pressure is defined as the point when the water flux reversely flows through the membrane. Both the pristine TFC and TFC-B-5 membranes have a burst pressure of 16 bar. Apparently, blending a small percentage (i.e., 5%) of the bulky *p*-xylylenediamine moiety into the TFC layer does not affect the burst pressure. However, the methanol treatment deteriorates the mechanical strength and lowers the burst pressure. Table 1 compares mechanical properties of PI-2 substrates before and after methanol treatment. Clearly, the tensile strength and Young's modulus decrease slightly, and lower the toughness of the swollen substrate. As a result, the TFC-MeOH membrane has a burst pressure of 13 bar (Figure 7) due to the weak mechanical properties of both the TFC layer and the substrate.

Figure 8 compares the evolution of water flux, reverse salt flux, and power density as a function of hydraulic pressure across the membrane in high pressure PRO processes. For all three TFC membranes, water flux declines with increasing hydraulic pressures because of the reduction in effective driving force ($\Delta\pi$-ΔP), while reverse salt flux increases and power density reaches a maximum and then falls. The TFC membrane has an initial water flux of 35.0 LMH and a reverse salt flux of 7.1 gMH at 0 bar. The water flux slowly goes down at low hydraulic pressures (0–6 bar) while the reverse salt flux smoothly increases. When the pressure is higher than 8 bar, the water flux progressively declines, and the reverse salt flux soars up to more than 100 gMH. In the case of the TFC-B-5 membrane, the water flux at 0 bar is higher than that of the pristine one. At low pressures, the water flux declines similarly to the pristine TFC membrane. However, a sharper decrease is observed under high pressures (i.e., 9–15 bar). Also, the reverse salt flux is higher than that of the pristine membrane.

The TFC-MeOH membrane shows the worst PRO performance under pressures even though it possesses the highest water flux of 43.7 LMH at 0 bar. As a result, the TFC-B-5 membrane holds the highest power density of 6.0 W/m^2, followed by the TFC membrane of 5.3 W/m^2, while the TFC-MeOH membrane has a lowest of 2.6 W/m^2. The different performance among these three membranes suggests that an increase in free volume may facilitate water permeation and improve PRO performance; however, a large increase in free volume may also promote salt passage, impair the selectivity of the TFC layer, and therefore, harm its PRO performance. In addition, swollen membranes may suffer from low mechanical strength as the swelling effect may result in the breakage of the weakly crosslinked polyamide molecules, leading to a low resistance to high pressures.

It has been brought to our attention that the high hydraulic pressures used in PRO tests may have some adverse effects on membranes, such as breakage/damage in the supporting layer, delamination between the supporting layer and TFC layer, or a deformed TFC polyamide structure.[34,35] Therefore, the transport properties of these three membranes are retested after PRO operations in order to examine the effects of high pressure. As shown in Table 3, the water permeability of each TFC membrane increases but its corresponding salt rejection reduces. However, no apparent damage and delamination are observed in their FESEM images for both TFC layer and substrate after PRO operations, as illustrated in Figure 9. Figure 8 also reconfirm the reproducibility of their PRO performance. As the variations of transport properties before and after PRO tests are products of structural deformation, defect formation, and chain package in the TFC layer, a slow positron beam is used to examine TFC membranes comprising PI substrates before and after the high pressure PRO tests.

Figure 10 shows the depth profiles of *S* parameter vs. positron incident energy for these three TFC membranes. There are three factors affecting the *S* parameter in polymers: (1) free-volume content (based on parapositronium (*p*-Ps) annihilation), (2) free-volume size (based on the uncertainty principle), and (3) chemical composition. The sharp ramp at the low positron energy range, which corresponds to the membrane surface and near surface, is probably attributed to the back diffusion and scattering of positronium.[43,50] Once the *S* parameter reaches the first peak of the TFC layer, it gradually decreases which indicates a transition change from the polyamide TFC layer to the PI substrate due to the quenching effect caused by the PI substrates. The VEPFIT fitting process works well with a three-layer model, and Figure 10 also gives the fitted thicknesses of TFC layers. The TFC layer thicknesses of the TFC, TFC-B-5, and TFC-MeOH membranes drop from 69 ± 21 to 58 ± 10 nm, from 57 ± 23 to 41 ± 14 nm, and from 52 ± 17 to 24 ± 6, respectively, after high pressure PRO tests. Consistent with permeability data, the TFC-MeOH membrane has the highest thickness reduction possibly due to the release of unreacted monomers during the methanol treatment[34,52,53] and imperfect chain recompaction during the PRO tests. As a result, the tested TFC-MeOH membrane shows the lowest intrinsic water permeability (Table 3) regardless of the dense layer thickness.

In addition, *S* parameters of all TFC layers drop after PRO operations. Clearly, all TFC layers obviously undergo

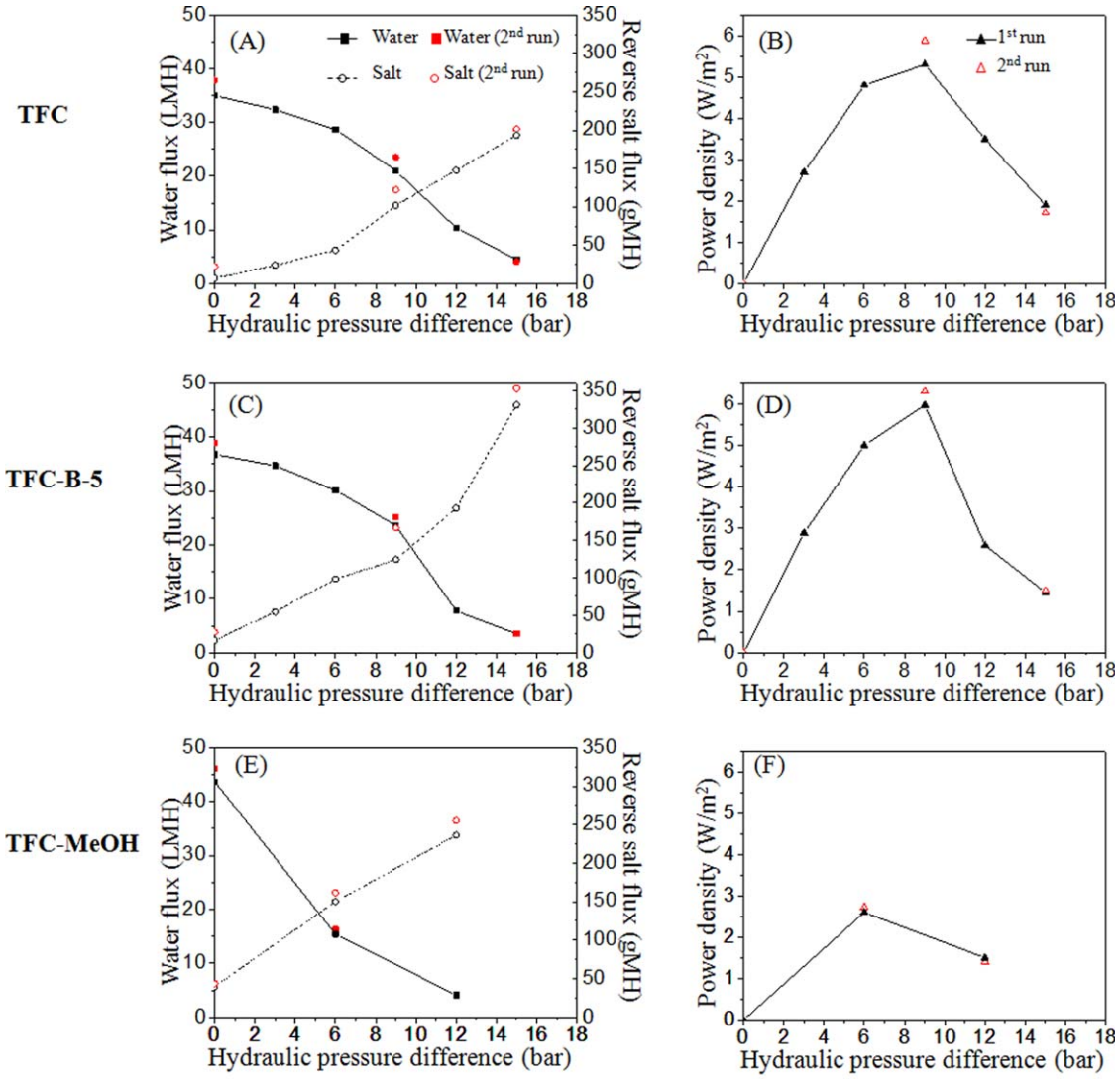

Figure 8. TFC membrane performance under high pressure PRO tests using deionized water as the feed solution and 1 M NaCl as the draw solution.

(A, C, E) Water flux and reverse salt flux, and (B, D, F) power density as a function of hydraulic pressure difference. The red dots are repeated data for the second run using the same membrane after PRO tests. [Color figure can be viewed in the online issue, which is available at wileyonlinelibrary.com.]

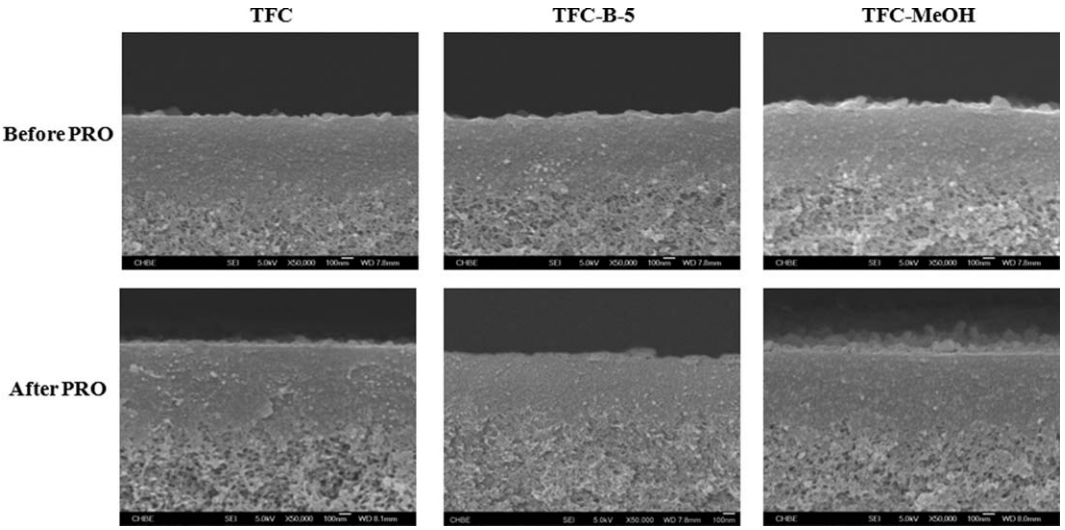

Figure 9. SEM images of top morphology before and after high pressure PRO processes for the three TFC membranes.

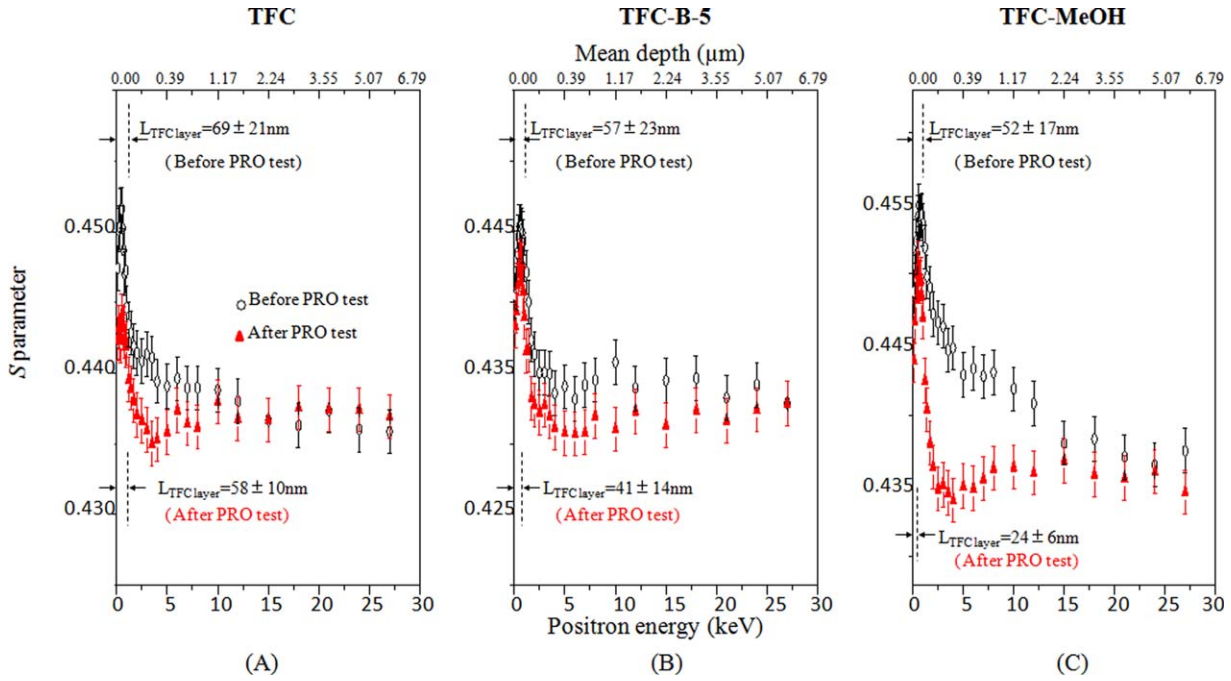

Figure 10. *S* parameter of (A) the TFC membrane, (B) the TFC-B-5 membrane, and (C) the TFC-MeOH membrane as a function of positron energy and mean depth before and after PRO tests.

[Color figure can be viewed in the online issue, which is available at wileyonlinelibrary.com.]

compaction during high pressure tests. A compacted free volume usually leads to a reduced permeability, but a smaller thickness facilitates the mass transfer and enhances water and salt permeabilities. Therefore, a thinner thickness may be the major cause for the variations of water and salt permeabilities after high pressure PRO tests. Imperfect chain packing in the TFC layer may also play a role to enhance water and salt permeabilities. Although the thinner TFC layers and imperfect chain recompaction are inevitable in PRO operations, they have limited adverse impact on membrane performance in terms of resistance to high pressures and power density.

Conclusions

We have molecularly designed TFC membranes with different free volumes and systematically studied the effects of free volume on osmotic power generation. A balance on (1) free volume, water flux, and reverse salt leakage of TFC layers and (2) mechanical properties of porous substrates is essential to design high-performance TFC membranes for PRO operations. By using P84 as the substrate material and monomers containing 5 mole % *p*-xylylenediamine for interfacial polymerization, the newly developed PRO TFC membrane displays a power density of 6.0 W/m^2 at 9 bar. The following conclusions can also be drawn from this work:

1. By adjusting the EG/PI ratio in casting solutions, one can manipulate the porous substrates with different physicochemical properties in terms of morphology, PWP, and mechanical properties, as well as TFC membranes with different morphology and FO performance.

2. The free volume of the TFC layer can be tailored by (a) blending of a bulky p-xylylenediamine monomer for interfacial polymerization and (b) conducting methanol treatment to induce swelling. The former slightly enlarges the free volume radius, whereas the latter greatly broadens the free volume cavity.

3. An increment in free volume promotes water and salt permeabilities as well as water and salt fluxes in FO processes; however, a large free volume enlargement may impair the selectivity of the TFC layer and make adverse impact on power generation.

4. The TFC layers become thinner and their free volume decreases during high pressure PRO operations, while both water and salt permeabilities increase but without compromising the power density.

Acknowledgments

This research was funded under the project entitled "Membrane development for osmotic power generation, Part 1. Materials development and membrane fabrication" (1102-IRIS-11-01) and NUS grant number of R-279-000-381-279. This research grant is supported by the Singapore National Research Foundation under its Environmental and Water Technologies Strategic Research Programme and administered by the Environment and Water Industry Programme Office (EWI) of the PUB. Thanks are due to Dr. Z.Z. Zhou, Miss. H. Wang, Mr. Y.P. Tang, Dr. S. Zhang, Dr. D.Y. Xing, Miss. R.C. Ong, and Miss J. Gao for their useful comments and suggestions.

Literature Cited

1. Chung TS, Li X, Ong RC, Ge QC, Wang HL, Han G. Emerging forward osmosis (FO) technologies and challenges ahead for clean water and clean energy applications. *Curr Opin Chem Eng*. 2012;1:246–257.
2. Kim J, Lee J, Kim JH. Overview of pressure-retarded osmosis (PRO) process and hybrid application to sea water reverse osmosis process. *Desalin Water Treat*. 2012;43:193–200.
3. Loeb S. Osmotic power plants. *Science*. 1975;189:654–655.
4. Loeb S. Production of energy from concentrated brines by pressure-retarded osmosis. I. Preliminary technical and economic correlations. *J Membr Sci*. 1976;1:49–63.

5. Loeb S, Mehta GD. A two-coefficient water transport equation for pressure-retarded osmosis. *J Membr Sci*. 1979;4:351–362.
6. Lee K, Baker R, Lonsdale H. Membranes for power generation by pressure-retarded osmosis. *J Membr Sci*. 1981;8:141–171.
7. Herron J. Asymmetric forward osmosis membranes. US Patent 7,445,712 B2, 2008; Available at: http://www.htiwater.com..
8. Gerstandt K, Peinemann K-V, Skilhagen SE, Thorsen T, Holt T. Membrane processes in energy supply for an osmotic power plant. *Desalination*. 2008;224:64–70.
9. Thorsen T, Holt T. The potential for power production from salinity gradients by pressure retarded osmosis. *J Membr Sci*. 2009;335:103–110.
10. Wang KY, Yang Q, Chung TS, Rajagopalan R. Enhanced forward osmosis from chemically modified polybenzimidazole (PBI) nanofiltration hollow fiber membranes with a thin wall. *Chem Eng Sci*. 2009;64:1577–1584.
11. Yang Q, Wang KY, Chung TS. Dual-layer hollow fibers with enhanced flux as novel forward osmosis membranes for water reclamation. *Environ Sci Technol*. 2009;43:2800–2805.
12. Hausman R, Digman B, Escobar IC, Coleman M, Chung TS. Functionalization of polybenzimidizole membranes to impart negative charge and hydrophilicity. *J Membr Sci*. 2010;363:195–203.
13. Wang KY, Ong RC, Chung TS. Double-skinned forward osmosis membranes for reducing internal concentration polarization within the porous sublayer. *Ind Eng Chem Res*. 2010;49:4824–4831.
14. Wang R, Shi L, Tang CY, Chou S, Qiu C, Fane AG. Characterization of novel forward osmosis hollow fiber membranes. *J Membr Sci*. 2010;355:158–167.
15. Zhang S, Wang KY, Chung TS, Chen H, Jean YC, Amy G. Well-constructed cellulose acetate membranes for forward osmosis: minimized internal concentration polarization with an ultra-thin selective layer. *J Membr Sci*. 2010;360:522–535.
16. Yip NY, Tiraferri A, Phillip WA, Schiffman JD, Elimelech M. High performance thin-film composite forward osmosis membrane. *Environ Sci Technol*. 2010;44:3812–3818.
17. Li X, Wang KY, Helmer B, Chung TS. Thin-film composite membranes and formation mechanism of thin-film layers on hydrophilic cellulose acetate propionate substrates for forward osmosis processes. *Ind Eng Chem Res*. 2012;51:10039–10050.
18. Qiu C, Qi S, Tang CY. Synthesis of high flux forward osmosis membranes by chemically crosslinked layer-by-layer polyelectrolytes. *J Membr Sci*. 2011;381:74–80.
19. Wang KY, Chung TS, Amy G. Developing thin-film-composite forward osmosis membranes on the PES/SPSf substrate through interfacial polymerization. *AIChE J*. 2012;58:770–781.
20. Widjojo N, Chung TS, Weber M, Maletzko C, Warzelhan V. The role of sulphonated polymer and macrovoid-free structure in the support layer for thin-film composite (TFC) forward osmosis (FO) membranes. *J Membr Sci*. 2011;383:214–223.
21. Han G, Chung TS, Toriida M, Tamai S. Thin-film composite forward osmosis membranes with novel hydrophilic supports for desalination. *J Membr Sci*. 2012;423–424:543–555.
22. Qin JJ, Liberman B, Kekre KA. Direct osmosis for reverse osmosis fouling control: principles, applications and recent developments. *Open Chem Eng J*. 2009;3:8–16.
23. Mi B, Elimelech M. Chemical and physical aspects of organic fouling of forward osmosis membranes. *J Membr Sci*. 2008;320:292–302.
24. Mi B, Elimelech M. Organic fouling of forward osmosis membranes: fouling reversibility and cleaning without chemical reagents. *J Membr Sci*. 2010;348:337–345.
25. Zou L, Vidalis I, Steele D, Michelmore A, Low SP, Verberk JQJC. Surface hydrophilic modification of RO membranes by plasma polymerization for low organic fouling. *J Membr Sci*. 2011;369:420–428.
26. Qin JJ, Lay WCL, Kekre KA. Recent developments and future challenges of forward osmosis for desalination: a review. *Desalin Water Treat*. 2012;39:123–136.
27. Chung TS, Zhang S, Wang KY, Su JC, Ling MM. Forward osmosis processes: yesterday, today and tomorrow. *Desalin*. 2012;287:78–81.
28. Zhao S, Zou L, Tang CY, Mulcahy D. Recent developments in forward osmosis: opportunities and challenges. *J Membr Sci*. 2012;396:1–21.
29. Phuntsho S, Shon HK, Hong S, Lee S, Vigneswaran S. A novel low energy fertilizer driven forward osmosis desalination for direct fertigation: evaluating the performance of fertilizer draw solutions. *J Membr Sci*. 2011;375:172–181.
30. Achilli A, Cath TY, Childress AE. Power generation with pressure retarded osmosis: an experimental and theoretical investigation. *J Membr Sci*. 2009;343:42–52.
31. Yip NY, Tiraferri A, Phillip WA, Schiffman JD, Hoover LA, Kim YC, Elimelech M. Thin-film composite pressure retarded osmosis membranes for sustainable power generation from salinity gradients. *Environ Sci Technol*. 2011;45:4360–4369.
32. Chou S, Wang R, Shi L, She Q, Tang CY, Fane AG. Thin-film composite hollow fiber membranes for pressure retarded osmosis (PRO) process with high power density. *J Membr Sci*. 2012;389:25–33.
33. She Q, Jin X, Tang CY. Osmotic power production from salinity gradient resource by pressure retarded osmosis: effects of operating conditions and reverse solute diffusion. *J Membr Sci*. 2012;401–402:262–273.
34. Zhang S, Fu FJ, Chung TS. Substrate modifications and alcohol treatment on thin film composite membranes for osmotic power. *Chem Eng Sci*. 2013;87:40–50.
35. Li X, Zhang S, Fu FJ, Chung TS. Deformation and reinforcement of thin-film composite (TFC) polyamide-imide (PAI) membranes for osmotic power generation. *J Membr Sci*. 2013;434:204–217.
36. Wang H, Liu S, Chung TS, Chen H, Jean YC, Pramoda KP. The evolution of poly(hydroxyamide amic acid) to poly(benzoxazole) via stepwise thermal cyclization: structural changes and gas transport properties. *Polymer*. 2011;52:5127–5138.
37. Coleman, P. Positron Beams and Their Applications. Singapore: World Scientific Publishing, 2000.
38. Jean YC, Mallon PE, Schrader DM. Principles and Applications of Positron and Positronium Chemistry. Singapore: World Scientific Publishing, 2003.
39. Huang YH, Chao WC, Hung WS, An QF, Chang KS, Huang SH, Tung KL, Lee KR, Lai JY. Investigation of fine-structure of polyamide thin-film composite membrane under swelling effect by positron annihilation lifetime spectroscopy and molecular dynamics simulation. *J Membr Sci*. 2012;417–418:201–209.
40. Zhang S, Zhang R, Jean YC, Paul DR, Chung TS. Cellulose esters for forward osmosis: characterization of water and salt transport properties and free volume. *Polymer*. 2012;53:2664–2672.
41. Ong RC, Chung TS, Helmer B, de Wit J. Novel cellulose esters for forward osmosis membranes. *Ind Eng Chem Res*. 2012;51:16135–16145.
42. McCutcheon JR, McGinnis RL, Elimelech M. Desalination by ammonia-carbon dioxide forward osmosis: influence of draw and feed solution concentrations on process performance, *J Membr Sci*. 2006;278:114–123.
43. Chen H, Hung WS, Lo CH, Huang SH, Cheng ML, Liu G, Lee KR, Lai JY, Sun YM, Hu CC, Suzuki R, Ohdaira T, Oshima N, Jean YC. Free-volume depth profile of polymeric membranes studied by positron annihilation spectroscopy: layer structure from interfacial polymerization. *Macromolecules*. 2007;40:7542–7557.
44. Shintani T, Shimazu A, Yahagi S, Matsuyama H. Characterization of methyl-substituted polyamides used for reverse osmosis membranes by positron annihilation lifetime spectroscopy and MD simulation. *J Appl Polym Sci*. 2009;113:1757–1762.
45. Kirkegaard P, Pederson NJ, Eldrup M. PATFIT-88: A Data Processing System for Positron Annihilation Spectra on Mainframe and Personal Computers. Roskilde, Denmark: Risoe National Laboratory, DK-4000, 1989.
46. Kim JH, Lee KH. Effect of PEG additive on membrane formation by phase inversion. *J Membr Sci*. 1998;138:153–163.
47. Krok M, Pamula E. Poly(L-lactide-co-glycolide) microporous membranes for medical applications produced with the use of polyethylene glycol as a pore former. *J Appl Polym Sci*. 2012;125:E187–E199.
48. Ali M, Zafar M, Jamil T, Butt MTZ. Influence of glycol additives on the structure and performance of cellulose acetate/zinc oxide blend membranes. *Desalination*. 2011;270:98–104.
49. Bridge MJ, Broadhead KW, Hlady V, Tresco PA. Ethanol treatment alters the ultrastructure and permeability of PAN-PVC hollow fiber cell encapsulation membranes. *J Membr Sci*. 2002;195:51–64.
50. Li FY, Li Y, Chung TS, Chen H, Jean YC, Kawi S. Development and positron annihilation spectroscopy (PAS) characterization of polyamide imide (PAI)–polyethersulfone (PES) based defect-free dual-layer hollow fiber membranes with an ultrathin dense-selective layer for gas separation. *J Membr Sci*. 2011;378:541–550.
51. Shao L, Chung TS, Goh SH, Pramoda KP. Transport properties of cross-linked polyimide membranes induced by different generations of diaminobutane (DAB) dendrimers. *J Membr Sci*. 2004;238:153–163.

52. Zuo J, Wang Y, Su SP, Chung TS. Molecular design of thin film composite (TFC) hollow fiber membranes for isopropanol dehydration via pervaporation. *J Membr Sci*. 2012;405:123–133.
53. Solomon MFJ, Bhole Y, Livingston AG. High flux hydrophobic membranes for organic solvent nanofiltration (OSN)-interfacial polymerization, surface modification and solvent activation. *J Membr Sci*. 2012;423:371–382.
54. Roh IJ, Park SY, Kim JJ, Kim CK. Effects of the polyamide molecular structure on the performance of reverse osmosis membranes. *J Polym Sci Part B: Polym Phys*. 1998;36:1821–1830.
55. La YH, Sooriyakumaran R, Miller DC, Fujiwara M, Terui Y, Yamanaka K, McCloskey BD, Freeman BD, Allen RD. Novel thin film composite membrane containing ionizable hydrophobes: pH dependent reverse osmosis behavior and improved chlorine resistance. *J Mater Chem*. 2010;20:4615–4620.
56. Nanda D, Tung KL, Hung WS, Lo CH, Jean YC, Lee KR, Hu CC, Lai JY. Characterization of fouled nanofiltration membranes using positron annihilation spectroscopy. *J Membr Sci*. 2011;382:124–134.
57. Shukla A, Peter M, Hoffmann L. Analysis of positron lifetime spectra using quantified maximum entropy and a general linear filter. *Nucl Instrum Methods Phys Res*. 1993;A335:310–317.
58. Geise GM, Lee HS, Miller DJ, Freeman BD, McGrath JE, Paul DR. Water purification by membranes: the role of polymer science. *J Polym Sci Part B: Polym Phys*. 2010;48:1685–1718.

Manuscript received Feb. 26, 2013, and revision received July 8, 2013.